Quantification of α-Synuclein Binding to Lipid Vesicles Using Fluorescence Correlation Spectroscopy

Elizabeth Rhoades,* Trudy F. Ramlall,† Watt W. Webb,* and David Eliezer†
*Applied and Engineering Physics, Cornell University, Ithaca, New York; and †Department of Biochemistry and Program in Structural Biology, Weill Medical College of Cornell University, New York, New York

ABSTRACT α-Synuclein (αS) is a soluble synaptic protein that is the major proteinaceous component of insoluble fibrillar Lewy body deposits that are the hallmark of Parkinson's disease. The interaction of αS with synaptic vesicles is thought to be critical both to its normal function as well as to its pathological role in Parkinson's disease. We demonstrate the use of fluorescence correlation spectroscopy as a tool for rapid and quantitative analysis of the binding of αS to large unilamellar vesicles of various lipid compositions. We find that αS binds preferentially to vesicles containing acidic lipids, and that this interaction can be blocked by increasing the concentration of NaCl in solution. Negative charge is not the only factor determining binding, as we clearly observe binding to vesicles composed entirely of zwitterionic lipids. Additionally, we find enhanced binding to lipids with less bulky headgroups. Quantification of the protein-to-lipid ratio required for binding to different lipid compositions, combined with other data in the literature, yields an upper bound estimate for the number of lipid molecules required to bind each individual molecule of αS. Our results demonstrate that fluorescence correlation spectroscopy provides a powerful tool for the quantitative characterization of αS-lipid interactions.

INTRODUCTION

α-Synuclein (αS) is the major fibrillar component of the Lewy body deposits in the *substantia nigra* that are characteristic of Parkinson's disease (PD) (1,2). Though the precise role of αS in the degeneration of dopaminergic neurons in PD remains unclear, the identification of two autosomal dominant mutations in αS that result in early onset PD established that it is critical to the progression of the disease state (3,4). More recently, a third αS mutation, as well as triplication of the αS gene, have also been linked to disease (5–8). α-Synuclein is a small, ~14.5 kDa, soluble protein that is found abundantly in presynaptic nerve terminals in various regions of the brain (9). The native function of αS is poorly understood, though it has been shown to affect dopamine synthesis (10–12) and transport (13), and it is thought that αS may play a role both in maintaining neuronal plasticity (14) and in the regulation of synaptic vesicle recycling (15). Despite these proposed functions, αS is only loosely associated with either the synaptic membrane or synaptic vesicles, often behaving as a soluble protein in brain tissue extracts (1,14).

Although αS is intrinsically unstructured in solution (16), it undergoes a conformational change to a predominantly α-helical structure upon association with lipid membranes (17,18). Sequence similarities between the N-terminus of αS and the lipid-binding domains of some classes of apolipoproteins led to the proposal that the N-terminus mediates αS interactions with membranes (16,18). This has been confirmed by NMR and EPR studies of αS bound to detergent micelles and small unilamellar vesicles (SUVs) (19–21), which show that the N-terminus forms an amphipathic helix (with an unusual 11/3 periodicity) upon association with micelles or vesicles, while the C-terminus remains largely free and unstructured (20,22). It has been suggested that the interaction of αS with membranes plays a role not only in the normal function of the protein but also in the pathology of PD. Specifically, studies have identified an oligomeric form of αS that is toxic to cells in culture (23), and shown that αS is capable of forming stable, porelike oligomers in vitro (24), leading to the postulation that αS oligomers may be responsible for permeabilization of cell membranes in the disease state (25–27).

There have been a number of in vitro studies aimed at elucidating the nature of the interaction of αS with membranes, using model synthetic lipid vesicles as well as extracted brain tissue lipids. However, much of the existing literature regarding these interactions is contradictory. The majority of studies indicate that αS binds preferentially to acidic phospholipids (17,18,28,29), though different affinities for specific phospholipid headgroups have been reported. In contrast, binding of αS to zwitterionic large unilamellar vesicles (LUVs) (30) and zwitterionic gel-phase SUVs (31) has also been described. Adding to the debate is the question as to whether or not association with lipids may inhibit (29,32) or promote (29,33–35) fibrillar αS formation.

The lack of general consensus regarding the nature of αS-lipid interactions may in part be due to experimental factors, including the long timescales needed for the commonly used techniques of gel filtration and gel electrophoresis, or

Submitted December 8, 2005, and accepted for publication March 13, 2006.

Address reprint requests to David Eliezer, Weill Medical College of Cornell University, Dept. of Biochemistry, 1300 York Ave., New York, NY 10021. Tel.: 212-746-6557; E-mail: dae2005@med.cornell.edu; or to Watt W. Webb, Cornell University, School of Applied & Engineering Physics, 212 Clark Hall, Ithaca, NY 14853-2501. Tel.: 607-255-3331; E-mail: www2@cornell.edu.

0006-3495/06/06/4692/09 $2.00

doi: 10.1529/biophysj.105.079251

the technical constraints of thin layer chromatography (17). Fluorescence correlation spectroscopy (FCS) allows for rapid, equilibrium characterization of solutions of fluorescently-labeled molecules. The potential for FCS as a powerful technique for studying the binding of peptides and proteins to LUVs has been demonstrated by a handful of studies (36–38). The work of Rusu et al. (37) studied the binding of a model peptide to LUVs, to allow for comparison between the binding parameters determined by FCS with those measured by other techniques. Using a well-characterized peptide-lipid system allowed them to evaluate the efficacy of FCS as a means of quantifying protein and peptide binding to phospholipid vesicles.

Here we report our studies of fluorescently-labeled αS binding to LUVs using FCS. We characterize the effects of vesicle composition and size, as well as the presence of monovalent and divalent ions, on the binding of αS to vesicles. In particular, we screen for affinity of αS for specific lipid headgroups to investigate the role of charge and packing density in determining binding.

MATERIALS AND METHODS

Protein expression and labeling

A plasmid containing a construct for wild-type αS (αS-wt) under control of the T7 promoter was generously provided by Dr. Peter Lansbury (Harvard Medical School). A serine-to-cysteine mutation was introduced at position 9 to allow for specific labeling of the protein (αS-S9C) using a QuikChange Site-Directed Mutagenesis kit (Stratagene, La Jolla, CA). Both αS-wt and αS-S9C were expressed and purified as described previously (19). The protein αS-S9C was labeled with AlexaFluor 488 C_5 maleimide dye (Molecular Probes, Invitrogen, Carlsbad, CA) generally according to the protocol provided by the manufacturer. Alexa 488 was chosen for the fluorophore based on its photophysical properties, including photostability, high quantum yield upon conjugation to αS, and large two-photon cross section (as characterized by the authors and colleagues). Briefly, the αS-S9C protein was dissolved in pH 6.4 phosphate-buffered saline and a 25 mM stock solution of the dye was prepared in dimethylsulfoxide and added to the protein solution to a final molar ratio of ~5:1 dye/protein. The protein-dye solution was incubated in the dark at room temperature for a minimum of 2 h and unreacted free dye was removed using Micro Bio-Spin 6 Chromatography columns (Bio-Rad, Hercules, CA). The labeled protein, αS-S9C-AL488, was passed through an additional spin column just before measurement to remove any residual free dye. The final protein concentrations and labeling efficiency were determined by absorption.

Preparation of vesicles

All vesicle components—1-palmitoyl-2-oleoyl-phosphatidylcholine (POPC), 1-palmitoyl-2-oleoyl-phosphatidylserine (POPS), 1-palmitoyl-2-oleoyl-phosphatidic acid (POPA), 1-palmitoyl-2-oleoyl-phosphoethanolamine (POPE), cholesterol, egg sphingomyelin, 1,2-dioleoyl-phosphocholine (DOPC), and 1,2-dioleoyl-phosphoethanolamine lissamine rhodamine (DOPE-rhod)—were purchased in lyophilized form from Avanti Polar Lipids (Birmingham, AL). Stock solutions of 10 mg/ml were prepared in chloroform and stored in sealed glass vials at −20°C. Stock solutions were assayed to determine actual concentrations before preparation of vesicles (39,40). Aliquots of the appropriate amounts of the stock solutions were mixed in clean glass vials and the chloroform was removed under a gentle stream of nitrogen. The lipids were placed under vacuum for at least 4 h to ensure complete removal of residual chloroform and then rehydrated in 50 mM sodium phosphate buffer, pH 7.4, to a final concentration of 2.5 or 5 mM lipid. Large unilamellar vesicles (LUVs) were prepared by repetitive extrusion through two layers of polycarbonate films in a handheld extruder (Avestin, Ottawa, Canada) (41). Vesicles were used within 2 days of preparation but were found to be structurally stable for at least two weeks when stored at 4°C. For vesicles composed of more than one type of lipid, all percentages of lipids are mole percentages. Unless specifically noted, LUVs refers to vesicles formed using 100 nm polycarbonate films.

Fluorescent vesicles were prepared by the addition of a small amount (~1:20,000 molar ratio labeled-lipid/total lipid) of labeled lipid, DOPE-rhod, to the stock solution.

Preparation of samples

Stock solutions of 10 μM protein were prepared of αS-S9C-AL488 and αS-wt. The stock LUV solutions were first diluted to the desired concentration in 50 mM sodium phosphate buffer, pH 7.4, then αS, S9C-AL488 or wt, was added. The samples were mixed by gently pipeting the solutions several times and then immediately transferred to sample chambers for measurements.

Measurements were made in eight-chambered Lab-Tek cover-glass slides (Nunc, Rochester, NY). The chambers were treated by plasma cleaning and then incubated with polylysine-conjugated polyethylene glycol to prevent adhesion of αS to the surfaces (42). The chambers were then incubated with low concentrations of aqueous POPC solutions. The chambers were rinsed thoroughly with HPLC H_2O before placing the sample in the chambers. Chambers that were not used immediately were filled with HPLC water, which was removed just before filling chambers with sample. There was no evidence of either vesicles or αS adsorbing to the chamber surfaces.

Principles of fluorescence correlation spectroscopy

Although FCS was invented more than 30 years ago (43–45), relatively recent improvements in computation, optical, and detection technologies (46) have made it a versatile technique that is widely used for a vast array of biochemical and biophysical characterization. The measured parameter in FCS is the spectrum of spontaneous fluctuations in fluorescence intensity caused by the changes in the emission of fluorescently-labeled molecules in the optically defined focal volume due to diffusion or chemical kinetics (Fig. 1 *A*). The concentration and the diffusion time of the diffusing species can be calculated from the autocorrelation function of the fluctuations. The diffusion time-scales linearly with the hydrodynamic radius of the diffusing species.

The autocorrelation function $G(\tau)$ is defined as

$$G(\tau) = \left\langle \frac{\partial F(0)\partial F(\tau)}{F(\tau)^2} \right\rangle, \tag{1}$$

where $F(\tau)$ is the fluorescence obtained from the volume at delay time τ and $\delta F(\tau) = F(\tau) - \langle F(\tau)\rangle$. The autocorrelation curves are fit with the standard formula for a three-dimensional multicomponent fit (47),

$$G(\tau) = \sum_i \frac{1}{N_i}\left[1 + \frac{\tau}{\tau_{Di}}\right]^{-1}\left[1 + \frac{\tau}{\omega^2\tau_{Di}}\right]^{-\frac{1}{2}}, \tag{2}$$

where N_i is the number of molecules of species i, τ_{Di} the characteristic diffusion time of species i, and ω is the ratio of the axial/radial dimensions of the observation volume. For a single diffusing species, $i = 1$, the equation is simply

$$G(\tau) = \frac{1}{N}\left[1 + \frac{\tau}{\tau_D}\right]^{-1}\left[1 + \frac{\tau}{\omega^2\tau_D}\right]^{-\frac{1}{2}}. \tag{3}$$

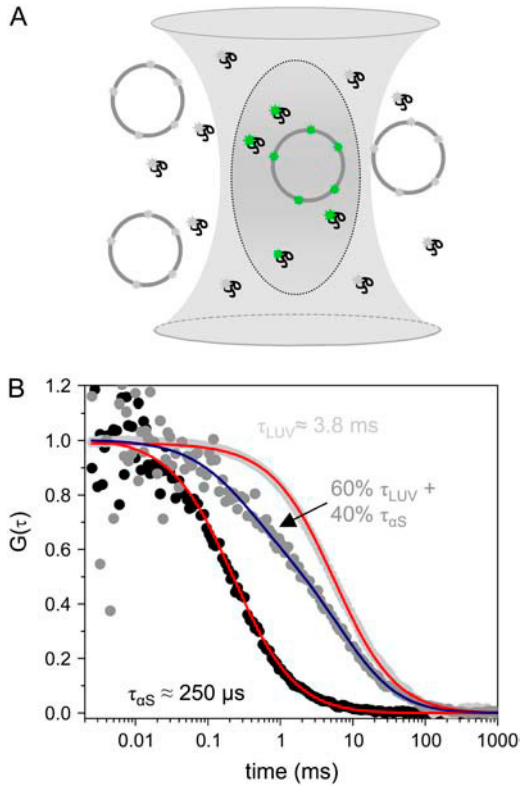

FIGURE 1 (*A*) Cartoon depicting the optically defined focal volume of an FCS instrument. Fluctuations in the intensity of the fluorescence signal result from the diffusion of the fluorescent molecules—shown here as free protein and LUV-bound protein—in and out of the focal volume. (*B*) Autocorrelation curves of αS only (*black*) and LUV only (*light gray*) are fit to Eq. 3 (fits in *red*); the autocorrelation curve of a mixture of free αS and LUV-bound αS (*dark gray*) is fit to Eq. 4 (fit in *blue*) to yield 60% LUV-bound αS and 40% free αS. The free αS has a diffusion time of ~250 μs and the ~120 nm LUVs have a diffusion time of ~3.8 ms, ~15 times longer than that of the free protein. This difference in diffusion times allows for separation of the contribution of each type of molecule in a mixed solution to the autocorrelation curve.

For a two-component system, such as that consisting of free αS and LUV-bound αS, the correlation function becomes

$$G(\tau) = \frac{1}{N}\left(f * \left[1 + \frac{\tau}{\tau_{\alpha S}}\right]^{-1}\left[1 + \frac{\tau}{\omega^2\tau_{\alpha S}}\right]^{-\frac{1}{2}} + (1-f) * \left[1 + \frac{\tau}{\tau_{LUV}}\right]^{-1}\left[1 + \frac{\tau}{\omega^2\tau_{LUV}}\right]^{-\frac{1}{2}}\right), \quad (4)$$

where f is the fraction of the signal that comes from free αS, $\tau_{\alpha S}$ is the characteristic diffusion time of free αS, and τ_{LUV} is the characteristic diffusion time of the vesicles. Because of the considerable difference in size between free αS and LUV-bound αS (Fig. 1 *B*), the contribution of each species to the correlation function can easily be distinguished by fitting the experimental data to Eq. 4.

Two-photon excitation fluorescence correlation spectroscopy

FCS measurements with two-photon excitation were made on an instrument assembled in our lab as described previously (48). Briefly, a pulsed-IR titanium-sapphire laser (Tsunami, Spectra-Physics, Palo Alto, CA) with 80 MHz, ~100-fs pulse-width was used as the excitation source, $\lambda = 895$ nm. The laser was directed into a 1.2 NA, 63× objective (Zeiss, Jena, Germany) mounted in an inverted microscope (Axiovert 35, Zeiss). The excitation power at the objective was between 1 and 4 mW, low enough to ensure that no photobleaching of the fluorophores occurred during their residence in the focal volume. Fluorescence emission was collected through the objective, separated from the excitation beam with a 670-nm longpass dichroic filter (Chroma, Rockingham, VT), and focused onto the face of a GaAsP photomultiplier tube (model No. H-7421, Hamamatsu, Somerville, NJ). The signal from the photomultiplier was autocorrelated by a digital correlator (ALV-6000, ALV, Langen, Germany). A typical data set consisted of 10 autocorrelation curves of 10 s each. These 10 curves were averaged and the average curve was fit according to Eqs. 3 or 4 using the standard deviation as a weighting factor.

Rhodamine green, a dye whose diffusion parameters have been well characterized by FCS (summarized in (49)), was measured as a calibration standard to determine ω, in Eqs. 2–4 above. Fitting autocorrelation curves of rhodamine green gives rise to $\omega = 3.4$. This value was then fixed for all subsequent fitting. Steady-state fluorescence (data not shown) was used to determine a quantum yield ratio of ~1 for free αS-S9C-AL488 relative to that of LUV-bound αS-S9C-AL488, and thus there was no need for correction of the fractions of free and LUV-bound protein as determined by Eq. 4.

RESULTS

FCS measurements of free αS and dye-labeled vesicles in separate experiments were used to determine their individual diffusion times. Fig. 1 *B* shows the autocorrelation curves of αS-S9C-AL488 and DOPE-rhod-labeled vesicles, as well as a curve with both free and LUV-bound αS-S9C-AL488 components. The curves for free αS and the LUVs were fit to Eq. 3, resulting in diffusion times of ~250 μs for the protein and ~3.8 ms for the vesicles. Both curves were well fit to single-component equations indicating monodisperse solutions. The corresponding hydrodynamic radius of ~60 nm, or diameter of ~120 nm, calculated for the vesicles is within the reported range of diameters for vesicles formed by extrusion through 100 nm pores. We saw some small variations in τ_{LUV}, depending upon the composition of the vesicles and the amount of protein bound; thus for the fitting of autocorrelation curves of solutions containing both free αS and LUV-bound αS using Eq. 4, $\tau_{\alpha S}$ was fixed to 250 μS, while τ_{LUV} was allowed to float to obtain the best fit for the data.

The placement of the Alexa 488 label was carefully chosen based on NMR-derived models of αS-micelle and αS-SUV interactions (20) to minimize possible disruption of protein-lipid interactions, and prior NMR studies confirmed that the S9C mutation does not significantly perturb the structure of detergent micelle-bound αS (22). Nevertheless, the possibility remained that the dye would affect—either negatively or positively—the binding of αS to the vesicles. To control for this, we made three samples containing 100% POPS LUVs with a fixed overall concentration of αS, but with varying relative amounts of αS-S9C-AL488 and αS-wt. The normalized autocorrelation curves (Fig. 2) are virtually indistinguishable, and fitting of the curves yields a fraction LUV-bound protein of ~0.8 for all three cases (Table 1).

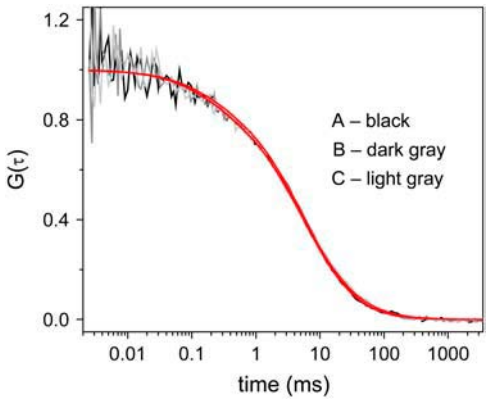

FIGURE 2 Autocorrelation curves of solutions with three different ratios of αS-S9C-AL488 and αS-wt for the same total concentration αS. (*A*) 200 nM αS-S9C-AL488 and 200 nM αS-wt. (*B*) 100 nM αS-S9C-AL488 and 300 nM αS-wt. (*C*) 50 nM αS-S9C-AL488 and 350 nM αS-wt. The fits to Eq. 4 of the three curves are shown in red. The curves are normalized to a $G(0) = 1$ to allow for comparison of the data.

Therefore, the wild-type and dye-labeled proteins appear to bind to the vesicles equally well. We also measured solutions of free Alexa 488 dye mixed with high (mM) concentrations of POPC and POPS LUVs and found no evidence of interactions of the free dye with the LUVs, as seen by autocorrelation curves that fit to a single diffusing component identical to that of free Alexa 488 dye in buffer (data not shown).

Because of significant experimental evidence that the presence of acidic phospholipid increases binding of αS to vesicles, 100% POPS LUVs were used for initial characterization of lipid binding by αS. Shown in Fig. 3 *A* are autocorrelation curves for a fixed amount of lipid (25 μM), a fixed amount of αS-S9C-AL488 (25 nM), and increasing amounts of αS-wt to increase the overall concentration of αS. FCS data were collected at each concentration of protein, and the autocorrelation curves were fit to Eq. 4 to yield the relative amounts of LUV-bound and free αS. For the initial data points where the concentration of αS is low, almost all of the protein is bound to the vesicles, but as the concentration of protein is increased past saturation, increasing amounts of free protein are found in the solution (Fig. 3 *A*, *inset*). This is shown not only by the fitting results, which indicate a decreasing fraction of LUV-bound protein, but also by the decrease in $G(0)$, which is inversely proportional to the average number of molecules in the focal volume, with increasing αS.

TABLE 1 Fraction of bound αS for each of the αS combinations shown in Fig. 2

Sample	αS-S9C-AL488	αS-wt	Fraction bound
A	250 nM	150 nM	0.796 ± 0.04
B	100 nM	300 nM	0.823 ± 0.035
C	25 nM	375 nM	0.784 ± 0.062

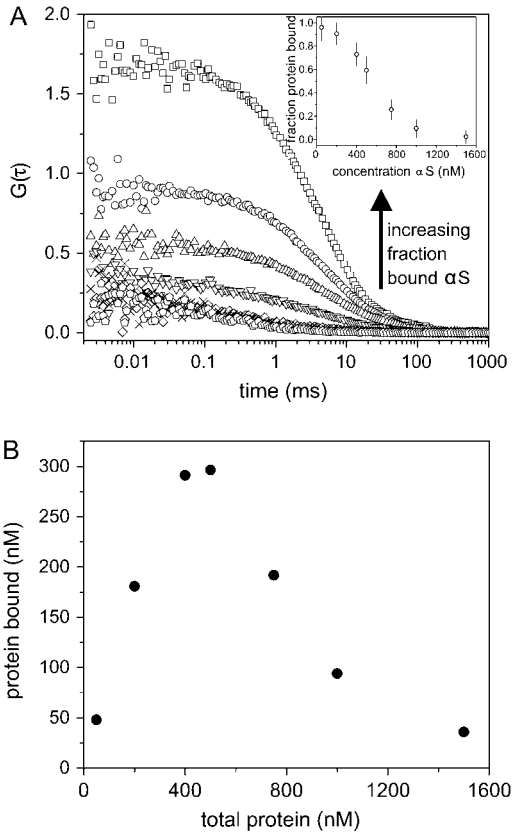

FIGURE 3 (*A*) Autocorrelation curves of solutions with increasing concentration of αS with 25 μM 100% POPS LUVs. The concentrations of αS shown are: 50 nM (*squares*), 200 nM (*circles*), 400 nM (*triangles*), 500 nM (*inverted triangles*), 750 nM (*diamonds*), 1 μM (*cross-hairs*), and 1.5 μM (*pentagons*) (the last three concentrations are difficult to differentiate on this plot). (*Inset*) The curves in panel *A* were fit with Eq. 4 to determine the fraction of free and bound αS. Increasing the αS concentration beyond saturation results in a decrease in the fraction of bound protein. (*B*). The data in Fig. 4 *A*, inset, is replotted as LUV-bound αS as a function of total αS. Above ~500 nM total αS, the total amount of bound protein begins to decrease instead of remaining constant as may be expected.

Surprisingly, when the data from Fig. 3 *A*, inset, are plotted as the concentration of LUV-bound protein versus the total protein concentration (Fig. 3 *B*), it becomes apparent that above a certain total protein concentration (~500 nm in this case) the concentration of LUV-bound protein starts to decrease instead of remaining constant as expected. The maximum amount of LUV-bound protein is observed at a protein/lipid mol ratio of ~1:45. At higher protein concentrations, more lipids are required per bound protein molecule. This is inconsistent with the saturation of a fixed number of protein binding sites on the lipid vesicles, and suggests instead that binding sites are eliminated at high protein/lipid ratios. α-Synuclein has been reported to destabilize lipid bilayers, and it may be that such an effect is responsible for these observations.

To investigate the role of the negatively charged lipids in binding, LUVs composed of various ratios of zwitterionic

POPC and acidic POPS were prepared. For each LUV composition, FCS data were collected at increasing LUV concentrations, while maintaining a constant αS concentration (200 nM), and the autocorrelation curves were fit to Eq. 4 to yield the relative amounts of LUV-bound and free αS. The fraction of LUV-bound protein calculated from FCS data was plotted as a function of the accessible lipid concentration, which is estimated to be half of the total lipid concentration, because it is assumed that αS cannot access the lipid of the interior of the vesicles. The data (Fig. 4 *A*) show that αS binds much more readily to LUVs containing a higher percentage of negatively charged lipids, in agreement with the majority of other in vitro lipid-binding studies. The binding curves are not hyperbolic and could not be well fit based on a simple partition equilibrium model. Data points collected at low lipid concentrations may be affected by the high protein/lipid ratio, as observed above, and may be partially responsible for the apparent lag in protein binding.

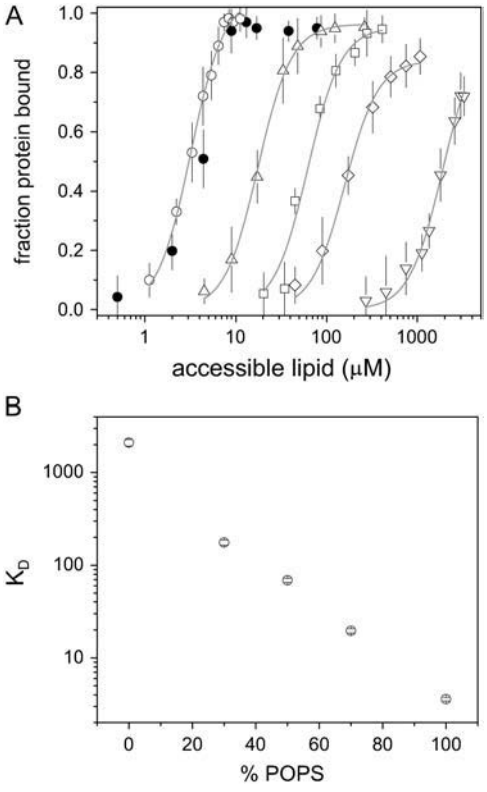

FIGURE 4 (*A*) Fraction αS bound as a function of lipid concentration for five different vesicle compositions. The concentration of αS was maintained at 200 nM, whereas the concentration of lipid was increased. The fraction αS bound was calculated from fitting Eq. 4 to the autocorrelation curves for each concentration of lipid: 100% POPS (*circles*), 70% POPS/30% POPC (*triangles*), 50% POPS/50% POPC (*squares*), 30% POPS/70% POPC (*diamonds*), and 100% POPC (*inverted triangles*). Also shown is the binding curve for ~60 nm diameter 100% POPS vesicles (*solid circles*). The fits shown in shaded representation are to the Hill equation, which yields a Hill coefficient ≈2.4 and a K_D for each composition of lipids. (*B*) The log of K_D as determined from the fits of the Hill equation to binding curves shown in panel *A* as a function of molar percentage POPS.

This effect has also been noted in a recent study using calorimetry to monitor the binding of αS to SUVs (31). This same study also noted that electrostatic interactions between the protein and the lipid vesicles lead to deviations from a simple partition equilibrium. Both of these effects might be expected to be mitigated at lower protein concentrations, but binding curves from data collected at a 10-fold lower concentration of αS (20 nM) showed the same shape and were also poorly fit by the partition equilibrium model (data not shown).

Reasonable fits to the binding curves could be obtained using the Hill equation and yielded apparent disassociation constants, K_D, for the various lipid compositions (Fig. 4 *B*). Similar K_D values were obtained either from best fits to a simple partition equilibrium or from 50% binding values extracted from best fits to a dose-response model. The apparently exponential relationship between K_D and the fraction of acidic lipid is predicted by Boltzmann and electrostatic theory (50). The value of the Hill coefficient obtained from the binding curves was ~2.4, but it is not clear how to interpret this value.

To further examine the role of charge-charge interactions in the binding of αS to lipids, increasing amounts of NaCl were added to a fixed amount of LUV and αS-S9C-AL488. As the concentration of NaCl was increased from 0 to 400 mM, the fraction of LUV-bound αS decreased (Fig. 5), showing that high salt concentrations inhibit lipid binding by αS. We also investigated the ability of the divalent ion calcium to disrupt αS-vesicle interactions. Due to the mutual insolubility of phosphate and calcium, the LUVs were made in 20 mM MOPS buffer, pH 7.4, rather than the standard phosphate buffer. Amounts of up to 20 mM $CaCl_2$, well above the physiologically relevant concentrations, had no effect on the binding of αS to the vesicles (data not shown).

The strong preference of αS for acidic phospholipids, as well as the decrease in its binding to 100% POPS vesicles with increasing NaCl concentrations, demonstrates the

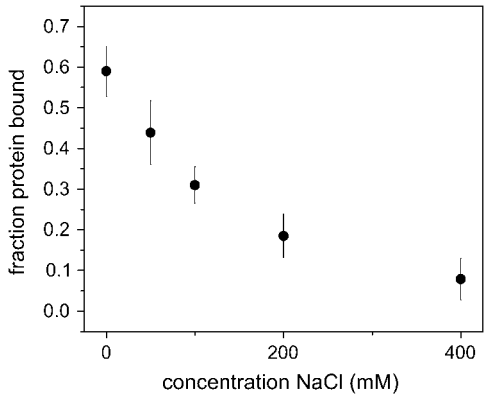

FIGURE 5 Fraction αS bound to 100% POPS LUVs as a function of NaCl concentration, with 200 nM αS. Increasing concentration of NaCl results in screening of the favorable electrostatic interactions between αS and the vesicles, and thus a decreasing fraction of bound protein.

importance of electrostatics in this interaction. However, binding to neutral POPC vesicles was also clearly observed and indicates that nonelectrostatic interactions are also involved. To investigate possible preferences of αS for specific phospholipid headgroups, three different combinations of acidic and zwitterionic lipids, each in a 1:1 molar ratio, were characterized at three different αS-S9C-AL488/lipid ratios (Fig. 6). Under conditions where less than half of the αS is bound to POPS/POPC, nearly 100% of the αS was bound to the POPA/POPC vesicles. The fraction of LUV-bound αS was also slightly higher for POPS/POPE vesicles than for POPS/POPC vesicles, indicating a preference for this composition—although the difference was much smaller than that observed for the POPA/POPC vesicles.

Because curvature has been suggested to play an important role in binding of αS to lipids (18), 100% POPS vesicles were prepared using polycarbonate membranes with a 50-nm pore size. The measured diffusion time corresponds to vesicles with a diameter of ~60 nm, or approximately one-half the diameter of the larger LUVs. The fraction of αS bound as a function of total accessible lipid for these vesicles is very close to the data obtained using the 120 nm 100% POPS LUVs (*solid* and *open circles* in Fig. 4 *A*, respectively), indicating no substantial preference on the part of αS for the more highly curved surface of the smaller vesicles.

Lastly, synaptic vesicles contain a high proportion of sphingomyelin and cholesterol, suggesting a propensity for phase heterogeneity in the membrane, a phenomenon that is thought to underlie the formation of raft domains in cellular membranes. Several recent articles have indicated localization of αS to lipid rafts in cells (51) or binding of αS with LUVs containing raft-associated components (52,53). Thus, we prepared LUVs corresponding to the canonical raft mixture of 1:1:1 molar ratio DOPC/sphingomyelin/cholesterol, which mimics the composition of the outer leaflet of the plasma membrane (54), as well as 100% DOPC LUVs. In both cases, the vesicles are electrostatically neutral. The fraction of LUV-bound αS for both types of LUVs was statistically indistinguishable from that found for 100% POPC vesicles (data not shown).

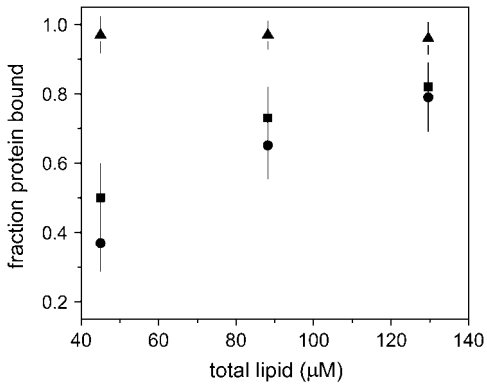

FIGURE 6 Comparison of fraction αS bound for three different combinations of lipids, with 200 nM αS. Each combination consists of a zwitterionic lipid and an acidic lipid in a 1:1 molar ratio: POPA/POPC (*triangles*), POPS/POPE (*squares*), and POPS/POPC (*circles*). The protein shows much stronger binding to the POPA/POPC and slightly stronger binding to POPS/POPE when compared to the POPS/POPC LUVs.

DISCUSSION

Using FCS to monitor αS-vesicle interactions

Although several other studies have established that FCS can be a powerful method for analyzing peptide and protein binding to LUVs (36–38), a primary goal of this study was to demonstrate the utility of FCS for quantifying binding of αS to lipid vesicles. FCS has several advantages over the techniques that have commonly been used to characterize αS-lipid interactions. A series of autocorrelation curves that allows for statistical analysis of the binding behavior can be collected within 2–3 min of first mixing the protein and vesicles together. This is in direct contrast to more traditional methods such as chromatography, where the protein and vesicles may spend several hours traversing a column or gel, or ultracentrifugation, which also requires several hours.

FCS is also applicable over a wide range of fluorophore concentrations, from nM to μM. For most of the experiments presented in this article, a fixed concentration of 200 nM αS-S9C-AL488 was used. However, the data shown in Fig. 3 were measured with 25 nM αS-S9C-AL488, and binding measurements using as little as 5 nM αS-S9C-AL488 were also performed (data not shown). This is between 100 and 1000 times lower protein concentration than is required for other techniques, such as circular dichroism (CD), chromatography, and calorimetry. Furthermore, as demonstrated in Fig. 3, the upper end of the range of protein concentrations can be extended almost indefinitely by maintaining the amount of fluorescently-labeled protein within the desired nM–μM range and adding unlabeled protein to achieve the desired final protein concentration, so long as the binding properties of the labeled and unlabeled proteins are the same (as we show to be the case here in Fig. 2).

CD is used to detect the binding of αS to lipids via the appearance of spectral lines associated with α-helical secondary structure (18), but quantitative interpretation of the results may not be straightforward. For example, a study by Jo et al. (17) found that although thin layer chromatography indicated binding of αS to POPE, POPE did not induce α-helical structure in αS as detected by CD unless an acidic lipid was also present. In another example, Narayanan and Scarlata (30) reported that interaction of αS with 100% POPS LUVs did not induce significant amounts of α-helical structure in αS according to their CD data. However, at αS concentrations above the saturating concentration, the primary component of the CD spectra comes from random-coil free αS with only a minor contribution arising from the small population of α-helical LUV-bound αS. In contrast, interpretation of binding data from FCS is straightforward,

because the signals from the free αS and LUV-bound αS are both detectable and separable, as well as being independent of secondary structure formation.

Lipid-binding properties of αS

Our data reveal a marked preference by αS for binding to acidic phospholipids (Fig. 4), consistent with a number of published studies. We also confirm that electrostatic interactions are important for αS-lipid binding, because physiological extracellular NaCl concentrations result in a considerable decrease, although not complete elimination, of the amount of αS bound to LUVs (Fig. 5). However, the data indicates a significantly higher affinity for vesicles composed of some portion of POPA over those containing an equivalent amount of POPS, as well as a slightly higher affinity for POPE over POPC (Fig. 6). Because both POPA and POPS are negatively charged and both POPE and POPC are zwitterionic, it appears that αS is sensitive to lipid headgroup properties beyond total charge. At pH 7.4, some percentage of POPA headgroups will have a valence of −2 (average relative charge ~−1.2 for POPA versus −1 for POPS at pH 7.4 (55)), which may partially account for the greater affinity of αS for POPA. In addition, POPA is lacking in the bulky amino-serine group of POPS, and might therefore be able to pack more closely together in a lipid bilayer, producing a higher charge density. Alternatively, the bulkier POPS headgroup may interfere sterically with αS binding. Several other studies have noted a preference for binding to POPA over POPS (18,28,56). This preference may be biologically relevant, because αS has been shown to regulate the activity of phospholipase D, an enzyme that produces PA from PC, and furthermore PA is a regulator of synaptic vesicle biogenesis, a process that may be affected by αS. However, it has also been pointed out that PS comprises ~7–12% of the total lipid in synaptic vesicles where αS localizes, whereas PA is only ~0–2% (18).

Our data provide a direct quantitation of the binding of αS to lipid vesicles. Fig. 3 *B* suggests that for POPS, the maximum achievable molar ratio of bound protein to total lipid is ~1:85, corresponding to a weight ratio of bound protein to total lipid of ~1:5. The POPS data in Fig. 4 *A* also show that complete protein binding can occur at a protein/total lipid molar ratio of ~1:100. For 1:1 POPA/POPC vesicles, Fig. 6 shows that complete binding can occur at a protein/lipid molar ratio of ~1:250. For 1:1 POPS/POPC, however, Fig. 4 *A* indicates that complete protein binding occurs at protein/lipid molar ratio of ~1:2000, corresponding to a weight ratio of bound protein to total lipid of ~1:100. However, it is important to note that this number merely provides an upper bound on the number of lipid molecules required to bind each αS molecule, since, in these experiments, the protein concentration is held fixed and might not be high enough to saturate every binding site. It is instructive to compare these results with other published work. An early study of αS lipid binding showed, using ultracentrifugation, that for 1:1 POPA/POPC vesicles, a 1:20 protein/lipid weight ratio (corresponding to a molar ratio of ~1:370) sufficed for complete protein binding, but the same ratio of protein to 1:1 POPS/POPC vesicles was insufficient for complete binding (18). These results are in good agreement with our own. Another early study reported that for 1:1 POPS/POPC vesicles, a protein/lipid weight ratio of 1:10 (corresponding to a molar ratio of ~1:185) was sufficient for complete protein binding as determined by CD data (17). A similar result was obtained for 1:1 POPG/POPC vesicles by another group (31). These studies were performed at higher protein concentrations (~10 μM) than our own (~200 nM), and this may account for the lower observed number of lipid molecules per bound protein molecule. In total, our results combined with those of others suggest that each molecule of αS can bind to a lipid bilayer patch composed of ≤85 acidic lipid molecules. Dilution of acidic lipids with neutral lipids significantly reduces the affinity of αS for the lipid surface but appears unlikely to alter the number of lipids bound per αS molecule.

These conclusions can be evaluated in the context of our knowledge of the structure of lipid-bound αS. The protein binds to lipid surfaces through a highly helical conformation adopted by the N-terminal ~100 residues, while the acidic C-terminal tail of the protein remains free. A 100-residue helix would be ~15-nm long and 1-nm wide, and would therefore cover a surface area of 15 nm^2. In comparison, an individual lipid molecule in a bilayer occupies ~0.5 nm^2 of surface area. Therefore, a minimum of 30 surface-accessible lipid molecules, or a 60-molecule bilayer patch, would be required to bind a single αS molecule. Our data indicate that ~1.5 times this minimum number of lipid molecules is actually required per αS molecule and that trying to force a higher αS/lipid ratio may result in destabilization of the lipid bilayer. Interestingly, αS oligomers have been reported to permeabilize phospholipid vesicles (26), and this has been proposed as a general mechanism of toxicity for amyloid-forming proteins (57). It is possible that in the absence of sufficient lipid surface area, αS oligomerization may be facilitated (this has been referred to as the parking-problem) leading to lipid bilayer disruption. Such a mechanism might also provide a partial explanation for the cooperativity observed in the binding curves of Fig. 4. However, we do not have any direct evidence for such a mechanism at present.

Finally, our preliminary examination of the interaction of αS with vesicles containing cholesterol and sphingomyelin shows that αS exhibits the same binding affinity for vesicles composed of a raft mixture of lipids as for 100% DOPC vesicles, suggesting that it is the presence of negatively charged components—either protein/peptide or phospholipids—in the raft domain of the membrane, rather than any physical property of the lipid phase itself that influences the binding of the protein. Nuscher et al. (31) characterized the binding of αS to neutral gel phase SUVs and attributed the binding affinity both to the high curvature of the SUVs

and to the formation of lipid phase domains within the vesicles. It is therefore possible that further binding studies using gel phase or liquid-ordered phase SUVs, instead of the LUVs examined here, would reveal a higher propensity for αS binding. Because of the possible physiological relevance of the raft membrane composition, this remains an avenue for further exploration. It is possible that small changes in the proportions of the lipid components may result in dramatic differences in membrane heterogeneity and thus drastically affect αS binding. FCS provides a rapid, quantitative means of characterizing these interactions.

This work was supported in part by a CMBSTD grant of the W. M. Keck Foundation (to E.R.), National Institute of Biomedical Imaging and BioEngineering, National Institutes of Health grant No. 9 P41 EB001976 (to W.W.W.), National Institute on Aging, National Institutes of Health grant No. 1 R21 AG26650 (to W.W.W.), National Institute on Aging, National Institutes of Health grant No. AG19391 (to D.E.), and by a gift from Herbert and Ann Siegel (to D.E.).

REFERENCES

1. Ueda, K., H. Fukushima, E. Masliah, Y. Xia, A. Iwai, M. Yoshimoto, D. A. C. Otero, J. Kondo, Y. Ihara, and T. Saitoh. 1993. Molecular cloning of CDNA—encoding an unrecognized component of amyloid in Alzheimer disease. *Proc. Natl. Acad. Sci. USA*. 90:11282–11286.
2. Goedert, M. 2001. Alpha-synuclein and neurodegenerative diseases. *Nat. Rev. Neurosci.* 2:492–501.
3. Kruger, R., W. Kuhn, T. Muller, D. Woitalla, M. Graeber, S. Kosel, H. Przuntek, J. T. Epplen, L. Schols, and O. Riess. 1998. $Ala_{30}Pro$ mutation in the gene encoding α-synuclein in Parkinson's disease. *Nat. Genet.* 18:106–108.
4. Polymeropoulos, M. H., C. Lavedan, E. Leroy, S. E. Ide, A. Dehejia, A. Dutra, B. Pike, H. Root, J. Rubenstein, R. Boyer, E. S. Stenroos, S. Chandrasekharappa, A. Athanassiadou, T. Papapetropoulos, W. G. Johnson, A. M. Lazzarini, R. C. Duvoisin, G. DiIorio, L. I. Golbe, and R. L. Nussbaum. 1997. Mutation in the α-synuclein gene identified in families with Parkinson's disease. *Science.* 276:2045–2047.
5. Zarranz, J. J., J. Alegre, J. C. Gomez-Esteban, E. Lezcano, R. Ros, I. Ampuero, L. Vidal, J. Hoenicka, O. Rodriguez, B. Atares, V. Llorens, E. G. Tortosa, T. del Ser, D. G. Munoz, and J. G. de Yebenes. 2004. The new mutation, E46K, of α-synuclein causes Parkinson and Lewy body dementia. *Ann. Neurol.* 55:164–173.
6. Bradbury, J. 2003. Alpha-synuclein gene triplication discovered in Parkinson's disease. *Lancet Neurol.* 2:715.
7. Singleton, A. B., M. Farrer, J. Johnson, A. Singleton, S. Hague, J. Kachergus, M. Hulihan, T. Peuralinna, A. Dutra, R. Nussbaum, S. Lincoln, A. Crawley, M. Hanson, D. Maraganore, C. Adler, M. R. Cookson, M. Muenter, M. Baptista, D. Miller, J. Blancato, J. Hardy, and K. Gwinn-Hardy. 2003. Alpha-synuclein locus triplication causes Parkinson's disease. *Science.* 302:841.
8. Farrer, M., J. Kachergus, L. Forno, S. Lincoln, D. S. Wang, M. Hulihan, D. Maraganore, K. Gwinn-Hardy, Z. Wszolek, D. Dickson, and J. W. Langston. 2004. Comparison of kindreds with Parkinsonism and α-synuclein genomic multiplications. *Ann. Neurol.* 55:174–179.
9. Clayton, D. F., and J. M. George. 1998. The synucleins: a family of proteins involved in synaptic function, plasticity, neurodegeneration and disease. *Trends Neurosci.* 21:249–254.
10. Lee, F. J. S., F. Liu, Z. B. Pristupa, and H. B. Niznik. 2001. Direct binding and functional coupling of α-synuclein to the dopamine transporters accelerate dopamine-induced apoptosis. *FASEB J.* 15:916–926.
11. Wersinger, C., D. Prou, P. Vernier, and A. Sidhu. 2003. Modulation of dopamine transporter function by α-synuclein is altered by impairment of cell adhesion and by induction of oxidative stress. *FASEB J.* 17:2151–2153.
12. Wersinger, C., and A. Sidhu. 2003. Attenuation of dopamine transporter activity by α-synuclein. *Neurosci. Lett.* 340:189–192.
13. Lotharius, J., S. Barg, P. Wiekop, C. Lundberg, H. K. Raymon, and P. Brundin. 2002. Effect of mutant α-synuclein on dopamine homeostasis in a new human mesencephalic cell line. *J. Biol. Chem.* 277:38884–38894.
14. George, J. M., H. Jin, W. S. Woods, and D. F. Clayton. 1995. Characterization of a novel protein regulated during the critical period for song learning in the Zebra Finch. *Neuron.* 15:361–372.
15. Lotharius, J., and P. Brundin. 2002. Impaired dopamine storage resulting from α-synuclein mutations may contribute to the pathogenesis of Parkinson's disease. *Hum. Mol. Genet.* 11:2395–2407.
16. Weinreb, P. H., W. G. Zhen, A. W. Poon, K. A. Conway, and P. T. Lansbury. 1996. NACP, a protein implicated in Alzheimer's disease and learning, is natively unfolded. *Biochemistry.* 35:13709–13715.
17. Jo, E. J., J. McLaurin, C. M. Yip, P. St George-Hyslop, and P. E. Fraser. 2000. Alpha-synuclein membrane interactions and lipid specificity. *J. Biol. Chem.* 275:34328–34334.
18. Davidson, W. S., A. Jonas, D. F. Clayton, and J. M. George. 1998. Stabilization of α-synuclein secondary structure upon binding to synthetic membranes. *J. Biol. Chem.* 273:9443–9449.
19. Eliezer, D., E. Kutluay, R. Bussell, and G. Browne. 2001. Conformational properties of α-synuclein in its free and lipid-associated states. *J. Mol. Biol.* 307:1061–1073.
20. Bussell, R., and D. Eliezer. 2003. A structural and functional role for 11-mer repeats in α-synuclein and other exchangeable lipid binding proteins. *J. Mol. Biol.* 329:763–778.
21. Jao, C. C., A. Der-Sarkissian, J. Chen, and R. Langen. 2004. Structure of membrane-bound α-synuclein studied by site-directed spin labeling. *Proc. Natl. Acad. Sci. USA.* 101:8331–8336.
22. Bussell, R., T. F. Ramlall, and D. Eliezer. 2005. Helix periodicity, topology, and dynamics of membrane-associated α-synuclein. *Protein Sci.* 14:862–872.
23. Rochet, J. C., T. F. Outeiro, K. A. Conway, T. T. Ding, M. J. Volles, H. A. Lashuel, R. M. Bieganski, S. L. Lindquist, and P. T. Lansbury. 2004. Interactions among α-synuclein, dopamine, and biomembranes—some clues for understanding neurodegeneration in Parkinson's disease. *J. Mol. Neurosci.* 23:23–33.
24. Volles, M. J., S. J. Lee, J. C. Rochet, M. D. Shtilerman, T. T. Ding, J. C. Kessler, and P. T. Lansbury. 2001. Vesicle permeabilization by protofibrillar α-synuclein: implications for the pathogenesis and treatment of Parkinson's disease. *Biochemistry.* 40:7812–7819.
25. Lashuel, H. A., B. M. Petre, J. Wall, M. Simon, R. J. Nowak, T. Walz, and P. T. Lansbury. 2002. Alpha-synuclein, especially the Parkinson's disease-associated mutants, forms pore-like annular and tubular protofibrils. *J. Mol. Biol.* 322:1089–1102.
26. Lashuel, H. A., D. Hartley, B. M. Petre, T. Walz, and P. T. Lansbury. 2002. Neurodegenerative disease—amyloid pores from pathogenic mutations. *Nature.* 418:291.
27. Conway, K. A., S. J. Lee, J. C. Rochet, T. T. Ding, R. E. Williamson, and P. T. Lansbury. 2000. Acceleration of oligomerization, not fibrillization, is a shared property of both α-synuclein mutations linked to early-onset Parkinson's disease: implications for pathogenesis and therapy. *Proc. Natl. Acad. Sci. USA.* 97:571–576.
28. Perrin, R. J., W. S. Woods, D. F. Clayton, and J. M. George. 2000. Interaction of human α-synuclein and Parkinson's disease variants with phospholipids—structural analysis using site-directed mutagenesis. *J. Biol. Chem.* 275:34393–34398.
29. Zhu, M., J. Li, and A. L. Fink. 2003. The association of α-synuclein with membranes affects bilayer structure, stability, and fibril formation. *J. Biol. Chem.* 278:40186–40197.
30. Narayanan, V., and S. Scarlata. 2001. Membrane binding and self-association of α-synucleins. *Biochemistry.* 40:9927–9934.

31. Nuscher, B., F. Kamp, T. Mehnert, S. Odoy, C. Haass, P. J. Kahle, and K. Beyer. 2004. Alpha-synuclein has a high affinity for packing defects in a bilayer membrane—a thermodynamics study. *J. Biol. Chem.* 279: 21966–21975.

32. Zhu, M., and A. L. Fink. 2003. Lipid binding inhibits α-synuclein fibril formation. *J. Biol. Chem.* 278:16873–16877.

33. Zhao, H. X., E. K. J. Tuominen, and P. K. J. Kinnunen. 2004. Formation of amyloid fibers triggered by phosphatidylserine-containing membranes. *Biochemistry.* 43:10302–10307.

34. Cole, N. B., D. D. Murphy, T. Grider, S. Rueter, D. Brasaemle, and R. L. Nussbaum. 2002. Lipid droplet binding and oligomerization properties of the Parkinson's disease protein α-synuclein. *J. Biol. Chem.* 277:6344–6352.

35. Lee, H. J., C. Choi, and S. J. Lee. 2002. Membrane-bound α-synuclein has a high aggregation propensity and the ability to seed the aggregation of the cytosolic form. *J. Biol. Chem.* 277:671–678.

36. Dorn, I. T., K. R. Neumaier, and R. Tampe. 1998. Molecular recognition of histidine-tagged molecules by metal-chelating lipids monitored by fluorescence energy transfer and correlation spectroscopy. *J. Am. Chem. Soc.* 120:2753–2763.

37. Rusu, L., A. Gambhir, S. McLaughlin, and J. Radler. 2004. Fluorescence correlation spectroscopy studies of peptide and protein binding to phospholipid vesicles. *Biophys. J.* 87:1044–1053.

38. Takakuwa, Y., C. G. Pack, X. L. An, S. Manno, E. Ito, and M. Kinjo. 1999. Fluorescence correlation spectroscopy analysis of the hydrophobic interactions of protein 4.1 with phosphatidyl serine liposomes. *Biophys. Chem.* 82:149–155.

39. Fiske, C. H., and Y. Subbarow. 1925. The colorimetric determination of phosphorus. *J. Biol. Chem.* 66:375–400.

40. Chen, P. S., T. Y. Toribara, and H. Warner. 1956. Microdetermination of phosphorus. *Anal. Chem.* 28:1756–1758.

41. Macdonald, R. C., R. I. Macdonald, B. P. M. Menco, K. Takeshita, N. K. Subbarao, and L. R. Hu. 1991. Small-volume extrusion apparatus for preparation of large unilamellar vesicles. *Biochim. Biophys. Acta.* 1061: 297–303.

42. Kenausis, G. L., J. Voros, D. L. Elbert, N. P. Huang, R. Hofer, L. Ruiz-Taylor, M. Textor, J. A. Hubbell, and N. D. Spencer. 2000. Poly(L-lysine)-*g*-poly(ethylene glycol) layers on metal oxide surfaces: attachment mechanism and effects of polymer architecture on resistance to protein adsorption. *J. Phys. Chem. B.* 104:3298–3309.

43. Magde, D., W. W. Webb, and E. Elson. 1972. Thermodynamic fluctuations in a reacting system—measurement by fluorescence correlation spectroscopy. *Phys. Rev. Lett.* 29:705–708.

44. Magde, D., E. L. Elson, and W. W. Webb. 1974. Fluorescence correlation spectroscopy. 2. Experimental realization. *Biopolymers.* 13:29–61.

45. Magde, D., and E. L. Elson. 1978. Fluorescence correlation spectroscopy. 3. Uniform translation and laminar-flow. *Biopolymers.* 17: 361–376.

46. Eigen, M., and R. Rigler. 1994. Sorting single molecules—application to diagnostics and evolutionary biotechnology. *Proc. Natl. Acad. Sci. USA.* 91:5740–5747.

47. Thompson, N. L. 1991. Fluorescence correlation spectroscopy. *In* Topics in Fluorescence Microscopy. J. Lakowicz, editor. Plenum Press, New York. 337–378

48. Larson, D. R., Y. M. Ma, V. M. Vogt, and W. W. Webb. 2003. Direct measurement of Gag-Gag interaction during retrovirus assembly with FRET and fluorescence correlation spectroscopy. *J. Cell Biol.* 162:1233–1244.

49. Hess, S. T., and W. W. Webb. 2002. Focal volume optics and experimental artifacts in confocal fluorescence correlation spectroscopy. *Biophys. J.* 83:2300–2317.

50. Arbuzova, A., L. B. Wang, J. Y. Wang, G. Hangyas-Mihalyne, D. Murray, B. Honig, and S. McLaughlin. 2000. Membrane binding of peptides containing both basic and aromatic residues. Experimental studies with peptides corresponding to the scaffolding region of caveolin and the effector region of MARCKS. *Biochemistry.* 39:10330–10339.

51. Fortin, D. L., M. D. Troyer, K. Nakamura, S. Kubo, M. D. Anthony, and R. H. Edwards. 2004. Lipid rafts mediate the synaptic localization of α-synuclein. *J. Neurosci.* 24:6715–6723.

52. Kubo, S., V. M. Nemani, R. J. Chalkey, M. D. Anthony, N. Hattori, Y. Mizuno, R. H. Edwards, and D. L. Fortin. 2005. A combinatorial code for the interaction of α-synuclein with membranes. *J. Biol. Chem.* 280:31664–31672.

53. Narayanan, V., Y. J. Guo, and S. Scarlata. 2005. Fluorescence studies suggest a role for α-synuclein in the phosphatidylinositol lipid signaling pathway. *Biochemistry.* 44:462–470.

54. Veatch, S. L., and S. L. Keller. 2002. Organization in lipid membranes containing cholesterol. *Phys. Rev. Lett.* 89:268101-1–268101-4.

55. Marsh, D. 1990. CRC Handbook of Lipid Bilayers. CRC Press, Boca Raton, FL.

56. Bussell, R., and D. Eliezer. 2004. Effects of Parkinson's disease-linked mutations on the structure of lipid-associated α-synuclein. *Biochemistry.* 43:4810–4818.

57. Bucciantini, M., E. Giannoni, F. Chiti, F. Baroni, L. Formigli, J. S. Zurdo, N. Taddei, G. Ramponi, C. M. Dobson, and M. Stefani. 2002. Inherent toxicity of aggregates implies a common mechanism for protein misfolding diseases. *Nature.* 416:507–511.